Top Catal (2011) 54:1403–1413
DOI 10.1007/s11244-011-9756-0

ORIGINAL PAPER

Enantiospecific Adsorption of (*R*)-3-Methylcyclohexanone on Naturally Chiral Surfaces Vicinal to Cu(110)

Ye Huang · Andrew J. Gellman

Published online: 20 October 2011

Abstract (*R*)-3-methylcyclohexanone (*R*-3MCHO) has been shown to adsorb enantiospecifically on naturally chiral Cu surfaces vicinal to the Cu(110) plane. Adsorption of *R*-3MCHO on seven Cu single crystal surfaces vicinal to (110) was studied using temperature programmed desorption. These surfaces include Cu(110), Cu(771), Cu(430), Cu(13,9,1)$^{R\&S}$ and Cu(651)$^{R\&S}$. The Cu(13,9,1)$^{R\&S}$ and Cu(651)$^{R\&S}$ surfaces are naturally chiral surfaces with terrace-step-kink structures. Enantioselective adsorption of *R*-3MCHO takes place on the chiral kink sites of these surfaces. Three *R*-3MCHO desorption features were resolved in the TPD spectra on Cu(13,9,1)$^{R\&S}$ and Cu(651)$^{R\&S}$ surfaces. Based upon comparisons between these and other Cu single crystal surfaces, they were assigned to desorption of *R*-3MCHO from flat terrace, close-packed step and kink sites. The desorption of *R*-3MCHO from the row and trough structure of the Cu(110) surface resembled desorption from a step structure rather than from a flat Cu(111) terrace. *R*-3MCHO desorbs enantiospecifically from the Cu(13,9,1)$^{R\&S}$ and Cu(651)$^{R\&S}$ surfaces. The peaks associated with *R*-3MCHO desorbing from the *R*- and *S*-chiral kink sites on Cu(13,9,1)$^{R\&S}$ differed in temperature by 2.4 ± 0.8 K. This corresponds to an enantiospecific difference in the desorption energies of 0.7 ± 0.2 kJ/mol, with a preference for *R*-3MCHO adsorption at the *R*-kinks. In contrast, *R*-3MCHO has a desorption energy from the *S*-kinks on the Cu(651)^{S} surface that is 0.7 ± 0.2 kJ/mol higher than from the *R*-kinks on the Cu(651)^{R} surface.

Keywords Copper single crystal · Chiral surface · Enantioselective adsorption · Temperature programmed desorption · Chiral adsorbate

Y. Huang · A. J. Gellman
Department of Chemical Engineering, Carnegie Mellon University, Pittsburgh, PA 15213, USA

A. J. Gellman (✉)
National Energy Technology Laboratory, U.S. Department of Energy, P.O. Box 10940, Pittsburgh, PA 15236, USA
e-mail: gellman@cmu.edu

1 Introduction

There is significant interest and impetus for the development of chiral surfaces for enantioselective chemical processing of chiral compounds. Chiral molecules have structures that are non-superimposable on their mirror images. The two non-superimposable forms are called enantiomers. Two enantiomers have identical chemical properties in an *achiral* environment, but are chemically differentiable in *chiral* environments such as living organisms. Enzymes are chiral and thus, living organisms will respond differently to the two enantiomers of chiral compounds that they have ingested. Because most pharmaceuticals are complex molecules, they have chiral structures. Thus, it is necessary to produce them in enantiomerically pure form, so that the therapeutically effective enantiomer can be administered without also administering the other enantiomer. This creates the need to develop and prepare chiral catalysts for the production of enantiomerically pure pharmaceuticals [1–3].

The most common way to prepare a chiral catalytic surface is to impart chirality to an achiral surface via adsorption of a chiral organic modifier [4–7]. Successful examples included the tartaric acid modified Ni-based catalysts [6] and cinchona alkaloid modified Pt-based catalysts [5]. Another route to preparing a chiral surface is to expose a low symmetry, high Miller index plane of an

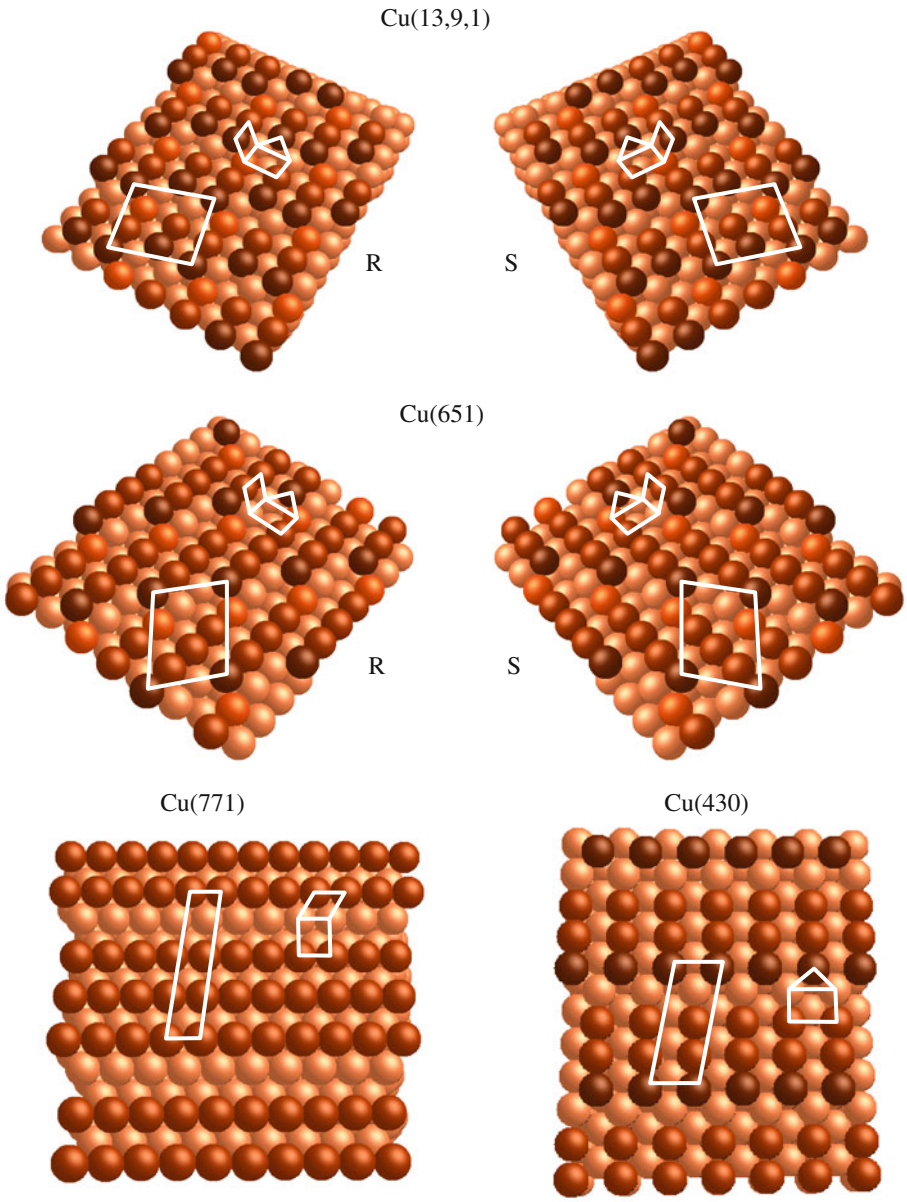

Fig. 1 Models of the ideally terminated Cu(13,9,1)$^{R\&S}$, Cu(651)$^{R\&S}$, Cu(771), and Cu(430) surfaces. The unit cell is superimposed on the figure, as are the low Miller index microfacets that intersect to form the kinks. The *different shading* of the Cu atoms indicates their different coordination numbers

achiral crystal lattice [8, 9]. Generally, such naturally chiral crystal surfaces are those that do not have mirror planes lying normal to the surface. For example, all surfaces of a face center cubic material having Miller indices (*hkl*), that satisfy the constraints $h \neq k \neq l \neq h$ and $h \cdot k \cdot l \neq 0$ are chiral [9]. These high Miller index chiral surfaces have structures composed of terrace, step and kink sites formed by microfacets of the three low Miller index planes [10]. The kink sites of these high Miller index surfaces provide a chiral environment for enantiospecific interactions with chiral adsorbates. A well studied example is the enantiospecific adsorption of chiral (*R*)-3-methylcyclohexanone (*R*-3MCHO) on Cu(643)$^{R\&S}$ surfaces [11–14]. *R*-3MCHO has been shown to adsorb at the kinks with an enantiospecific adsorption/desorption energy that is $\Delta\Delta E_{\mathrm{des}} = 0.97 \pm 0.25$ kJ/mol higher on the Cu(643)^{S} surface than on the Cu(643)^{R} surface. There are now many examples of enantiospecific surface chemistry on naturally chiral metal surfaces [8, 9, 12–32].

The focus of this paper is on the enantioselective adsorption of *R*-3MCHO on the chiral kink sites of Cu(13,9,1)$^{R\&S}$ and Cu(651)$^{R\&S}$ surfaces, probed by temperature programmed desorption (TPD). These surface are vicinal to the Cu(110) plane and are shown in Fig. 1. The white lines outline the unit cells of the ideal surface structures and outline the microfacets that form the motif used to describe the structures of these surfaces. Both Cu(13,9,1) and Cu(651) have (110) terraces but the Cu(13,9,1) surface has a (100) step and a (111) kink, while the Cu(651) surface has a (111) step and a (100) kink. Prior

work has revealed enantiospecific adsorption of *R*-3MCHO on the Cu(643)$^{R\&S}$ surfaces which are vicinal to the (111) plane and on the Cu(531)$^{R\&S}$ surfaces which lie at the center of the stereographic projection of fcc surfaces [11, 13, 14, 24]. To aid the interpretation of the desorption spectra of *R*-3MCHO from the Cu(13,9,1)$^{R\&S}$ and Cu(651)$^{R\&S}$ surfaces, three related Cu surfaces have also been studied: Cu(110), Cu(771) and Cu(430). The Cu(110) surface is not flat and has the same row and trough structure as the terraces on the Cu(13,9,1)$^{R\&S}$ and Cu(651)$^{R\&S}$ surfaces. The structures of Cu(771) and Cu(430) are shown in Fig. 1. Cu(771) has (110) terraces separated by straight, close-packed (111) steps, while Cu(430) has (110) terraces separated by (100) steps. These (100) steps are not close-packed. The *R*-3MCHO TPD spectra from the Cu(13,9,1)$^{R\&S}$ and Cu(651)$^{R\&S}$ surfaces exhibit features that can be assigned to desorption from these different structural features (flat terrace, close-packed step, and kink), and desorption from the chiral kinks has been shown to be enantiospecific.

2 Experimental

All experiments were conducted in a stainless steel ultra-high vacuum (UHV) chamber with a base pressure of 2×10^{-10} Torr. The UHV chamber was equipped with an Ar^+ ion sputtering gun to clean the surface, a low energy electron diffraction (LEED) optics to determine surface orientation and structure, and a quadrupole mass spectrometer to perform TPD. An X-ray photoemission spectrometer (XPS) was used to determine surface cleanliness.

The Cu single crystals (99.99% purity) were obtained from Monocrystals Company. The crystals were ~10 mm in diameter and ~2 mm thick. For the Cu(110), Cu(771) and Cu(430) surfaces, only one side was polished. For the chiral Cu(13,9,1)$^{R\&S}$ and Cu(651)$^{R\&S}$ surfaces, both sides of the crystal were polished. For these chiral surfaces, one side has the *R*-orientation and the other side has the *S*-orientation. The crystals were mounted between two tantalum wires spot-welded to their edges. The two tantalum wires were attached to a sample holder at the bottom of a UHV manipulator. The crystal could be cooled to ~80 K and heated resistively to over 1,000 K with the temperature measurement made using a chromel–alumel thermocouple spot-welded to the edge of the crystal.

The crystals were cleaned by cycles of Ar^+ ion sputtering (1.5 keV, 20 μA) and annealing to 1,000 K. The surface structures of crystals were verified by LEED. The handedness of the chiral surfaces were determined by X-ray diffraction (XRD) as described elsewhere [26].

R-3MCHO (98%) and racemic-3-methylcyclohexanone (rac-3MCHO, 97%) were purchased from the Aldrich Chemical Co. They were transferred as liquids to glass vials and subjected to several cycles of freezing, pumping, and thawing to remove impurities before exposing their vapor to the surface by introduction into the UHV chamber through a standard leak valve. The purity of the sample was verified by mass spectrometry. Exposures were reported in units of Langmuirs (L) and were not corrected for ion gauge sensitivities to different gas species.

The surfaces were cleaned by Ar^+ sputtering and annealing prior to each TPD experiment. TPD experiments were performed by first cooling the Cu sample with liquid nitrogen to ~80 K. 3MCHO was then adsorbed by exposure of the sample to 3MCHO vapor from a doser with the Cu sample held at a constant temperature. The Cu sample was held at different temperatures to control adsorption of 3MCHO at different sites on the surfaces, however, unless otherwise specified the adsorption temperature was ~80 K. Desorption measurements were performed by heating the Cu sample at a constant rate (1 K/s) while using the quadrupole mass spectrometer to monitor the species desorbing from the surface using the signal at $m/q = 69$. The fragmentation pattern of the desorbing species matches that of molecular 3MCHO. This has a number of fragments of which $m/q = 69$ yields the strongest signal and thus, the signal at $m/q = 69$ has been monitored during TPD experiments. Measurements comparing the 3MCHO desorption temperatures from the two different enantiomers of a chiral single crystal can have accuracies of ±0.5 K because these measurements are made on the opposite sides of the same crystal. Comparisons of desorption peak temperatures between different single crystals is not as accurate. The desorption temperatures of the *R*-3MCHO multilayer peaks, which ought to be very similar on all five single crystals, indicated an absolute accuracy of ±3 K for comparison of desorption temperature between different crystals.

3 Results

One of the nice features of the adsorption and desorption of *R*-3MCHO from Cu surfaces is that the resulting TPD spectra provide direct insight into the types of adsorption sites on the surface. Prior work has studied *R*-3MCHO desorption from the Cu(643) $^{R\&S}$ surfaces and a related set of surfaces vicinal to the Cu(111) plane [11, 14]. At monolayer coverage, the TPD spectra of *R*-3MCHO from the Cu(643)$^{R\&S}$ surfaces exhibit three distinct desorption peaks that can be assigned to molecules desorbing from the flat (111) terraces at 230 K, the straight close-packed (100) steps at 345 K and the (110) kinks at 385 K. Desorption from the *R*- and the *S*-kinks exhibits enantiospecificity; peak desorption temperatures differ by $\Delta T_p = 3.5 \pm 0.8$ K.

The TPD spectra of *R*-3MCHO from the surfaces vicinal to Cu(110), as reported in this paper, exhibit features similar to those observed from surfaces vicinal to (111) but with differences that are reflective of the details of the terrace, step and kink structure on these surfaces.

3.1 Coverage-Dependent Desorption of *R*-3MCHO from Cu(110)

In order to help in our understanding of the adsorption behavior on naturally chiral Cu(13,9,1)$^{R\&S}$ and Cu(651)$^{R\&S}$ surfaces, a few Cu surfaces with related structures were studied beforehand. Cu(110) is a high symmetry, achiral surface that has the structure of the microfacets forming the terraces on the Cu(13,9,1)$^{R\&S}$ and Cu(651)$^{R\&S}$ surfaces. Cu(771) and Cu(430) both have straight monoatomic steps separating (110) terraces, but the steps are of (111) and (100) orientation on Cu(771) and Cu(430), respectively (Fig. 1).

The Cu(110) surface is a high symmetry, nominally flat surface with a well known structure based on close-packed rows of atoms separated by troughs. Figure 2 shows the TPD spectra of *R*-3MCHO on Cu(110) after several

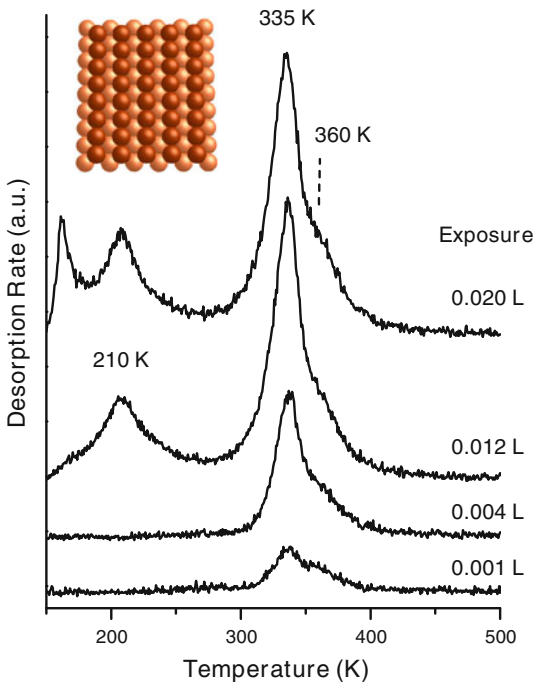

Fig. 2 TPD spectra of *R*-3MCHO on the Cu(110) surface following different initial exposures to *R*-3MCHO at 80 K. The exposure is in units of Langmuir (1 L = 1.0×10^{-6} Torr s). The primary desorption peak at 335 K is assigned to the desorption of *R*-3MCHO from some step-like sites which are the *straight close packed rows* of the Cu(110) structure. The desorption peak at ~210 K is assigned to the desorption of *R*-3MCHO from flat terrace sites that may arise from local faceting of the surface. The lowest temperature peak at ~163 K is assigned to desorption of the *R*-3MCHO multilayer

different initial exposures to *R*-3MCHO vapor with the Cu(110) surface at 80 K. At low exposures, the TPD spectra are dominated by a single feature with a peak desorption temperature of 335 K and a small high temperature shoulder at 360 K. At higher coverage, a second desorption feature appears at 210 K and upon saturation of the monolayer, the multilayer desorption feature appears at 163 K. The order in which these features appear as the exposure to *R*-3MCHO is increased is consistent with the sequential population of adsorption sites with decreasing binding energies for *R*-3MCHO.

The key difference between the *R*-3MCHO TPD spectra from Cu(111) and Cu(110) is that on the flat Cu(111) surface there is a single desorption feature at 230 K. On the Cu(643)$^{R\&S}$ surface, *R*-3MCHO has been shown to desorb from the (111) terraces, (100) steps and (110) kinks at 230, 345 and 385 K, respectively [13]. Evidence of all three features is apparent in the high coverage *R*-3MCHO TPD spectrum from Cu(110). The dominant feature at 335 K is suggestive of desorption from close-packed steps, rather than a flat terrace. Of course, in spite of the fact that the Cu(110) plane is a low Miller index plane and is often considered to be 'flat', it is not. Its structure is composed of close-packed rows separated by troughs, and to a molecule such as *R*-3MCHO this structure appears to be formed of straight, close-packed step edges. In fact, the surface structure classification system proposed recently by Jenkins and Pratt [33] suggests that 'flat' surfaces are those containing two or more close-packed rows of atoms whereas, surfaces such as Cu(110) that contain only one close-packed row are 'stepped'.

The feature at 360 K in the *R*-3MCHO TPD spectra from Cu(110) is reminiscent of desorption from kinks on the Cu(643) surface. It is possible that there are some number of atomic defects in the close-packed rows on the Cu(110) surface that expose adsorption sites that would appear to be kinks to adsorbed *R*-3MCHO. Alternately, it is possible that the adsorption of *R*-3MCHO can induce the formation of some kinks in the close-packed rows. Such adsorption induced kink formation has been observed in the case of room temperature adsorption of *R*-3MCHO on the Cu(221) and Cu(533) surfaces, both of which have structures based on (111) terraces separated by close-packed step edges [34].

Finally, the desorption feature at 210 K occurs at a temperature similar to that observed for *R*-3MCHO desorption from the flat Cu(111) surface. Although the clean Cu(110) surface is unreconstructed, many fcc(110) surfaces exhibit a (2 × 1) reconstruction which can be considered to arise from the formation of small (111) facets [35]. It is possible that at high coverages the adsorption of *R*-3MCHO induces the formation of some (111) facets giving rise to the desorption feature at 210 K. Alternatively,

some bunching of close-packed steps might result in the formation of flat terraces.

3.2 Coverage-Dependent Desorption of *R*-3MCHO from Cu(430)

The ideal structure of the Cu(430) surface has (110) terraces separated by (100) step edges (Fig. 1). One important distinction between the structure of the Cu(430) and the Cu(771) surface is that on the Cu(430) surface the (100) step edge is not close-packed. In the classification scheme proposed recently by Jenkins and Pratt [33], the Cu(430) surface would be considered 'kinked' rather than 'stepped'. It is important to point out that the Cu(430) surface does have a mirror plane perpendicular to the surface and thus, it is *achiral*, even if it is considered to be kinked.

The TPD spectra of *R*-3MCHO from the Cu(430) surface (Fig. 3) are quite distinct from those obtained from the Cu(110) surface. They are dominated at high temperature by two resolvable desorption features at 335 and 375 K. By analogy with our prior observations of *R*-3MCHO desorption from Cu(643), these would be assigned to desorption from straight, close-packed step edges and from kinks, respectively [11]. The distinction on Cu(430) is that these features arise from *R*-3MCHO desorption from the 'stepped' (110) terraces and the straight but kinked (100) step edge. Needless to say, one would not expect to observe enantiospecific desorption of chiral compounds from the kinked step edge on the Cu(430) surface because it is achiral.

The low temperature region of the *R*-3MCHO TPD spectrum from Cu(430) contains a broad desorption feature assignable to the presence of close packed (111) facets. At the highest coverage, multilayer desorption is observed at 160 K.

3.3 Desorption of *R*-3MCHO from Cu(*hkl*) at Monolayer Coverage

The surface structure dependent desorption kinetics of *R*-3MCHO illustrated above can be used to probe the structures of Cu surfaces vicinal to the (110) plane and to assign the desorption features observed from those surfaces. The *R*-3MCHO TPD spectra obtained from the Cu(110), Cu(771), Cu(430), Cu(13,9,1)^S and Cu(651)^R surfaces at monolayer coverage are shown in Fig. 4. In this instance, one monolayer is defined as the coverage at which the onset of multilayer desorption at $\sim$160 K is observed. The key desorption features exhibited in the spectra can be divided into three temperature regions: <300, 300–355, and >355 K. These can be assigned to desorption from terraces, steps, and kinks on these five surfaces in direct analogy to the assignment on the surfaces vicinal to Cu(111) [11–14]. As mentioned, the *R*-3MCHO TPD spectra from Cu(111) exhibits a single desorption feature at

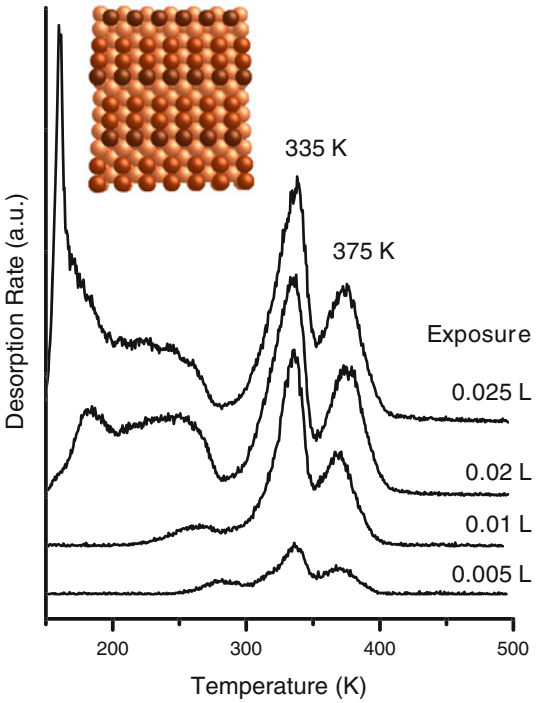

Fig. 3 TPD spectra of *R*-3MCHO on the Cu(430) surface following different initial exposures to *R*-3MCHO at 80 K. The high temperature desorption peak at 375 K is assigned to desorption from the kinked (100) step edge. The peak at 335 K is assigned to the stepped (110) terraces. The broad desorption peak at 200–275 K is assigned to desorption of *R*-3MCHO from flat terrace sites. The lowest temperature peak at 160 K is assigned to desorption of the *R*-3MCHO multilayer

230 K. The desorption spectra from Cu(221) and Cu(533) exhibit two features; one at 345 K associated with desorption from close packed step edges and another at $\sim$230 K associated with desorption from the flat (111) terraces. Finally, the desorption spectra from Cu(643) and Cu(653) exhibit three desorption features at 385, 345 and $\sim$230 K associated with desorption from kinks, straight steps edges and flat (111) terraces, respectively.

The *R*-3MCHO TPD spectra from the surfaces vicinal to (100) shown in Fig. 3 reveal features that can be classified using the same scheme as has been used for the surfaces vicinal to Cu(111); however, there are some interesting but easily rationalized differences. At the highest temperatures (>355 K), the Cu(13,9,1), Cu(651) and Cu(430) surfaces all show desorption peaks that are assigned to desorption from kinks. The Cu(13,9,1) and Cu(651) planes lie in the interior of the stereographic projection and are classified as kinked surfaces in most surface structure classification schemes. The unexpected feature is the desorption peak at 375 K from the Cu(430) surface. The Cu(430) plane lies on the perimeter of the stereographic triangle and is often classified as a stepped surface, rather than a kinked surface. However, inspection of the structure of the step edge on the Cu(430) surface reveals that it is not close-packed. In the

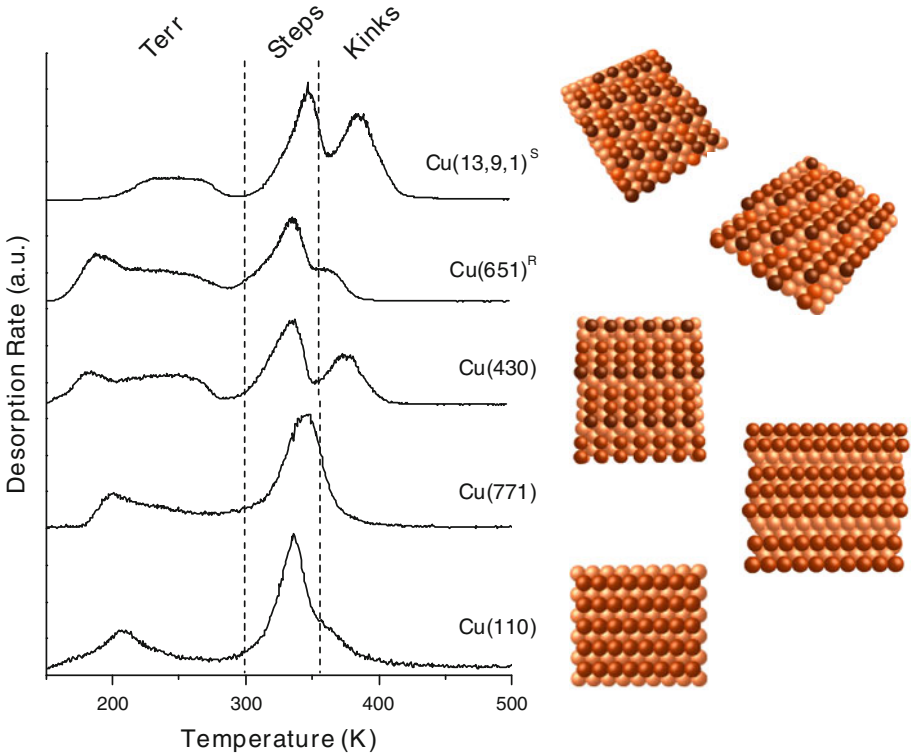

Fig. 4 TPD spectra of *R*-3MCHO from the Cu(110), Cu(771), Cu(430), Cu(651)^{R} and Cu(13,9,1)^{S} surfaces. All spectra were obtained at coverages of ~1 ML. The *dashed line* at 355 K denotes the boundary between desorption features associated with desorption from the straight close packed step edges (<355 K) and the features associated with desorption from kinks (>355 K). Desorption features at temperatures <300 K are associated with species desorbing from the flat terraces

classification scheme proposed by Jenkins and Pratt [33], the fact that this step edge is not close-packed would place Cu(430) into the category of *kinked* surfaces. In support of this classification scheme, the observation of a high temperature *R*-3MCHO desorption features at 375 K from the Cu(430) surface does suggest that its step edges are kinked. Of course, the fact that there is a mirror symmetry plane that lies perpendicular to the Cu(430) surface, running perpendicular to the non-close-packed steps, means that the kinks are not chiral.

Both the Cu(110) and the Cu(771) surfaces exhibit *R*-3MCHO desorption features in the temperature range 300–355 K associated with desorption from close-packed step edges. In the case of the Cu(771) surface, this is not surprising because its (110) terraces are separated by close-packed step edges (Figs. 1, 4). On the other hand, the Cu(110) surface is a low Miller index plane that is not commonly classified as being a stepped surface. However, Jenkins and Pratt [33] classify *stepped* surfaces as those with close-packed atomic rows running in only one direction. In their classification scheme, *flat* surfaces are those with close-packed rows running in two or more directions. Within this classification scheme, Cu(110) would be considered 'stepped' and from the point of view of its interaction with *R*-3MCHO it certainly exhibit step-like desorption features. In contrast, the desorption of *R*-3MCHO from the Cu(111) surface, which is flat, exhibits a single desorption feature at 230 K [11].

3.4 Enantiospecific Desorption of *R*-3MCHO from Cu(651)$^{R\&S}$

The Cu(651)$^{R\&S}$ surfaces are chiral and should, therefore, exhibits enantiospecific interactions with *R*-3MCHO. Enantiospecific adsorption of *R*-3MCHO on Cu(651)$^{R\&S}$ was studied by comparing the TPD spectra from both Cu(651)^{R} and Cu(651)^{S} surfaces and focusing on the TPD feature associated with desorption from the kinks. It is clear from the TPD spectra shown in Fig. 4 that the desorption features from the chiral kink sites are less intense than those from the step. Furthermore, the difference between the peak desorption temperatures from kinks and steps on the Cu(651)^{R} surface is far less than that between kinks and steps on the Cu(13,9,1)^{S} surface. As a result, at monolayer coverage, the TPD peaks arising from kinks and steps are not resolved on the Cu(651) surfaces. In order to minimize adsorption at the step sites and thus, resolve the peak arising from the kink sites, the substrate was kept at 320 K during exposure to *R*-3MCHO. Figure 5 shows TPD spectra obtained from the Cu(651)$^{R\&S}$ surfaces using this procedure. Because the substrate was kept at 320 K during exposure to *R*-3MCHO there is very little desorption from step sites. More importantly, it is possible to resolve the peak of the desorption feature arising from the kinks and to observe differences in the peak desorption temperatures from the Cu(651)^{R} and Cu(651)^{S} surfaces. The inset of Fig. 5 highlights the features associated with the desorption of

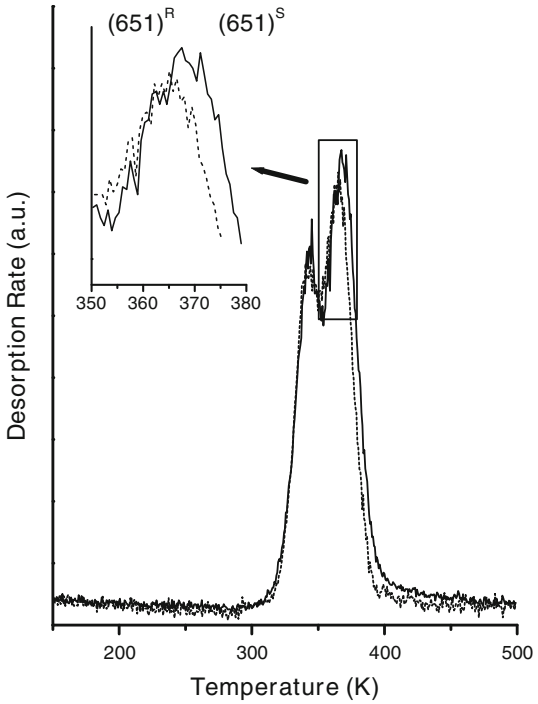

Fig. 5 TPD spectra of *R*-3MCHO on the Cu(651)$^{R\&S}$ surfaces. Both exposures are 0.30 L (1 L = 1.0×10^{-6} Torr s) with the surface held at 320 K. The desorption features from the kinks appear to be resolved from those attributed to straight steps. The *inset* shows the difference between the desorption peak temperatures of *R*-3MCHO on the *R*- and *S*-chiral kink sites of Cu(651)$^{R\&S}$. *R*-3MCHO has a higher adsorption energy at the kinks on the Cu(651)^{S} surface than at the kinks on the Cu(651)^{R} surface

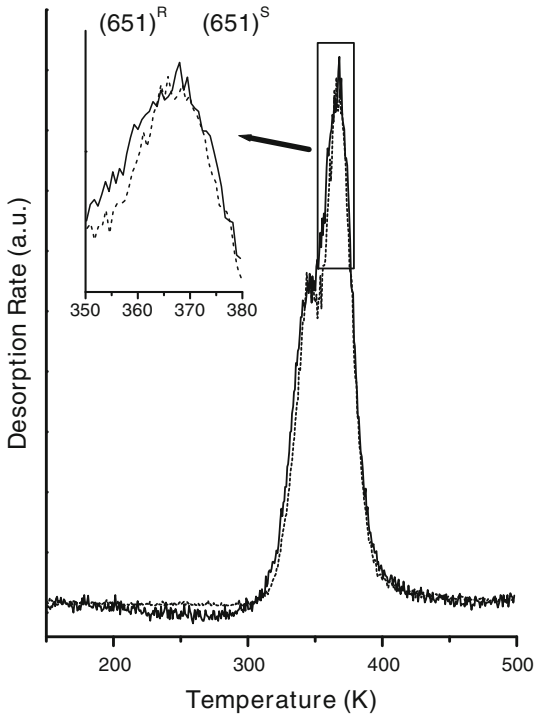

Fig. 6 TPD spectra of racemic 3-MCHO on the Cu(651)$^{R\&S}$ surfaces. Both exposures are 0.30 L (1 L = 1.0×10^{-6} Torr s) with the surface held at 320 K. The desorption features from the kinks appear to be resolved from those attributed to straight steps. The *inset* shows that there is no difference between the peak temperatures for racemic 3-MCHO desorption from the kinks of the Cu(651)$^{R\&S}$ surfaces

R-3MCHO from the chiral kink sites on Cu(651)$^{R\&S}$ surfaces. Five *R*-3MCHO TPD spectra were acquired from both Cu(651)^{R} and Cu(651)^{S} surfaces. All ten such TPD peaks have been fitted with Gaussian functions and the peak of the Gaussian fit has been used to determine the peak desorption temperature. The desorption of *R*-3MCHO from chiral kink sites occurs at $T_p^S = 367.5 \pm 0.6$ K on Cu(651)^{S} and $T_p^R = 365.1 \pm 0.4$ K on Cu(651)^{R} surfaces, a difference in desorption peak temperatures of $\Delta T_p = T_p^S - T_p^R = 2.4 \pm 0.7$ K. As was the case on the Cu(643)$^{R\&S}$ surfaces [11], *R*-3MCHO adsorbs preferentially on the *S*-kinks and desorbs at a higher temperature from the Cu(651)^{S} kinks than from the Cu(651)^{R} kinks.

If the differences in *R*-3MCHO desorption from the Cu(651)$^{R\&S}$ surfaces are truly due to enantiospecific interactions, then racemic 3MCHO (rac-3MCHO) should not exhibit any difference in its TPD spectra from the Cu(651)$^{R\&S}$ surfaces. As a control experiment, adsorption and desorption of rac-3MCHO was also studied on Cu(651)$^{R\&S}$ surfaces under the same conditions used to study desorption of *R*-3MCHO. The rac-3MCHO TPD spectra from Cu(651)^{R} and Cu(651)^{S} surfaces are compared in Fig. 6. The inset of Fig. 6 highlights the features associated with the desorption of rac-3MCHO from the chiral kink sites on Cu(651)$^{R\&S}$ surfaces. There is no significant difference between the peaks associated with rac-3MCHO desorption from the chiral kink sites on Cu(651)$^{R\&S}$ surfaces. Five rac-3MCHO TPD spectra were acquired from both Cu(651)^{R} and Cu(651)^{S} surfaces and used to determine the difference in the desorption temperatures on the two surfaces. The desorption of rac-3MCHO from chiral kink sites occurs at $T_p^S = 367.0 \pm 0.3$ K on Cu(651)^{S} and $T_p^R = 366.3 \pm 0.4$ K on Cu(651)^{R} surfaces. The difference between the two desorption temperatures is not significant. This control experiment indicates that the differences in *R*-3MCHO desorption from the Cu(651)$^{R\&S}$ surfaces are due to enantiospecific interactions with those surfaces.

3.5 Enantiospecific Desorption of *R*-3MCHO on Cu(13,9,1)$^{R\&S}$

The Cu(13,9,1)$^{R\&S}$ surfaces are chiral and should, therefore, exhibit enantiospecific interactions with *R*-3MCHO. The enantiospecific desorption of *R*-3MCHO from the Cu(13,9,1)$^{R\&S}$ surfaces was studied by comparing the TPD spectra obtained at monolayer coverage and focusing on the

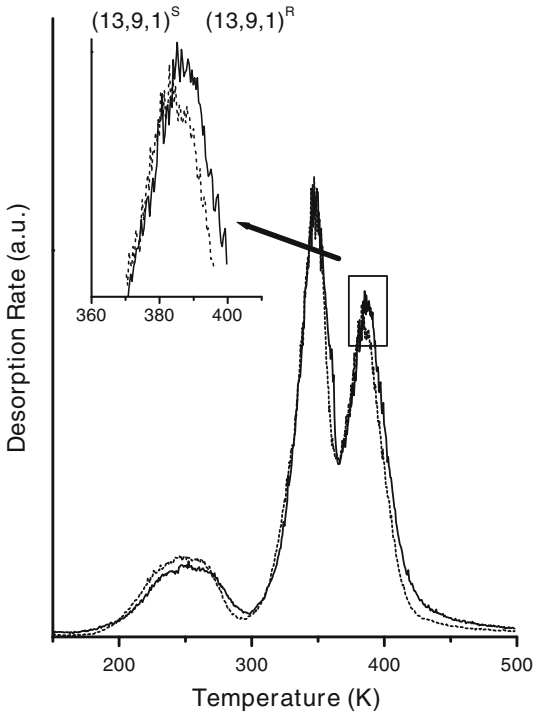

Fig. 7 TPD spectra of *R*-3MCHO on the Cu(13,9,1)$^{R\&S}$ surfaces. Both exposures are 0.30 L (1 L = 1.0×10^{-6} Torr s) with the surface held at 200 K. The three desorption features from flat terrace, straight step and kink sites appear in the spectra from both Cu(13,9,1)^{R} and Cu(13,9,1)^{S} surfaces. The *inset* shows the difference between the *R*-3MCHO desorption peaks on the *R*- and *S*-chiral kink sites of the Cu(13,9,1)$^{R\&S}$ surfaces. *R*-3MCHO has a higher adsorption energy at the kinks on the Cu(13,9,1)^{R} surface than at the kinks on the Cu(13,9,1)^{S} surface

TPD peak at ~385 K associated with desorption from the kinks. To ensure saturation of the adsorbed monolayer, the *R*-3MCHO exposure was 0.3 L and the substrate was kept at 200 K during exposure. Five TPD spectra were acquired from both the Cu(13,9,1)^{R} and Cu(13,9,1)^{S} surfaces. The TPD spectra in Fig. 7 exhibit similar desorption features associated with terrace, step and kink sites from both surfaces. The TPD peaks associated with desorption from straight, close-packed step edges occur at 345 K on both Cu(13,9,1)$^{R\&S}$ surfaces. The inset of Fig. 7 highlights the features associated with the desorption of *R*-3MCHO from the chiral kink sites on Cu(13,9,1)$^{R\&S}$ surfaces. It clearly reveals that *R*-3MCHO desorbs at higher temperatures from the chiral kink sites on Cu(13,9,1)^{R} surface than from the chiral kink sites on the Cu(13,9,1)^{S} surface. The desorption of *R*-3MCHO from chiral kink sites on Cu(13,9,1)^{R} occurs at $T_p^R = 386.4 \pm 0.5$ K but at $T_p^S = 384.0 \pm 0.6$ K on Cu(13,9,1)^{S}, a difference in desorption peak temperatures of $\Delta T_p = -2.4 \pm 0.8$ K. The magnitude of the enantiospecific peak temperature differences on the Cu(13,9,1)$^{R\&S}$ surfaces and the Cu(651)$^{R\&S}$ surfaces are the same, however, their sign is reversed.

The key difference between this result and the desorption temperature difference observed on the Cu(643)$^{R\&S}$ and Cu(651)$^{R\&S}$ surfaces is that on the Cu(13,9,1)$^{R\&S}$ surfaces, *R*-3MCHO adsorbs preferentially on the Cu(13,9,1)^{R} surface and desorbs at higher temperature than from Cu(13,9,1)^{S} whereas, on the Cu(643)$^{R\&S}$ and Cu(651)$^{R\&S}$ surfaces, *R*-3MCHO adsorbs preferentially on the *S*-surface [11, 13, 14]. The convention used for assignment of chirality to Cu(*hkl*)$^{R\&S}$ surfaces is based on the handedness of the rotational progression among the (111), (100) and (110) microfacets forming the kinks (Fig. 1); a clockwise progression is denoted *R*- and a counterclockwise progression is denoted *S*- [15, 17, 32]. The results of Figs. 5 and 7 demonstrate that the preference of *R*-3MCHO for adsorption at the chiral kink sites on the Cu(*hkl*)$^{R\&S}$ surfaces cannot be predicted using the convention used to assign surface chirality or handedness.

4 Discussion

Adsorption and desorption of *R*-3MCHO on seven Cu surfaces vicinal to the (110) plane has been investigated in order to look for evidence of enantioselectivity on the naturally chiral surfaces and to understand the influence of surface structure on enantioselective adsorption. In our prior study of adsorption and desorption on surfaces vicinal to the (111) plane, *R*-3MCHO proved to be an excellent probe of the types of adsorption sites exposed by these surfaces [11, 13, 14]. The same has held true on the surfaces vicinal to Cu(110) and, in addition, *R*-3MCHO has revealed some interesting features concerning their classification as *flat*, *stepped* or *kinked* surfaces. Furthermore, as a chiral adsorbate, *R*-3MCHO has served as a probe of enantiospecificity at the chiral kink sites on those surfaces with naturally chiral structures.

Adsorption and desorption of *R*-3MCHO from all Cu surfaces is reversible and thus, the desorption kinetics monitored in TPD experiments are reflective of adsorption energetics. On all seven surfaces, the coverage dependence of the *R*-3MCHO TPD spectra indicate roughly sequential population of adsorption sites with decreasing affinities for *R*-3MCHO adsorption. These sites are kinks with peak desorption temperatures in the range 360–385 K, closed-packed step edges with desorption temperatures in the range 335–350 K and flat terraces with desorption temperatures in the range 200–275 K. One of the interesting phenomenological observations made in the course of this work is that the Cu(110) surface should not be considered *flat*. Whereas, *R*-3MCHO desorption occurs at ~230 K on the flat, close-packed Cu(111) surface, it desorbs at 335 K on the Cu(110) surface, a temperature associated with desorption from close-packed step edges on the Cu(221)

and Cu(533) surfaces [11, 13, 14]. Given the fairly open, row and trough structure of the Cu(110) surface, perhaps this is not surprising; from the perspective of adsorbed *R*-3MCHO Cu(110) exposes a series of close-packed step edges. Similarly, the Cu(430) surface would normally be considered to be composed of straight (100) steps that separate (110) terraces. However, desorption of *R*-3MCHO occurs at 375 K which phenomenologically suggests the presence of kinks. Again, in hindsight this should not be too surprising given that the step edge on the Cu(430) surface is not close-packed. Thus, from the perspective of adsorbed *R*-3MCHO, the (100) step edge on Cu(430) exposes a row of kink sites. It is important to note that these kink sites have mirror symmetry and thus, they are achiral. These phenomenologically derived concepts of surface structure that are revealed by *R*-3MCHO desorption are, in fact, consistent with a surface classification scheme recently proposed by Jenkins and Pratt [33]. In that scheme, *flat* surfaces are those containing two or more close-packed atomic rows, *stepped* surfaces are those that contain only one close-packed row, and *kinked* surfaces are those containing no close-packed rows of atoms.

An alternative but related view of the origins of surface structure effects on *R*-3MCHO adsorption can be derived from considering the coordination of exposed atoms. The atoms in the flat Cu(111) surface and in the terraces of the surfaces vicinal to Cu(111) are all 9-fold coordinated. The atoms in the close packed step edges on the Cu(221), Cu(533) and Cu(771) surfaces are 7-fold coordinated. Similarly, the atoms in the rows on the Cu(110) surface are 7-fold coordinated. The dominant desorption feature of *R*-3MCHO on all four surfaces occurs at temperatures of 335–345 K. Finally, the least coordinated atoms on the Cu(13,9,1), Cu(651), Cu(643), Cu(653) and Cu(430) surfaces have 6-fold coordination. The highest temperature *R*-3MCHO desorption features on these surfaces all occur in the range 365–385 K. Clearly, there is a phenomenological relationship between the desorption temperatures or desorption energies on these surfaces and the coordination of the atoms that they expose.

Analysis of the *R*-3MCHO TPD spectra from the surfaces vicinal to Cu(110) and Cu(111) has been limited to the establishment of an empirical correlation between the observed desorption peaks and the types of adsorption sites exposed. In principle, one might consider an analysis of the peak areas to try to quantify the areal density of different sites on the surfaces; however, there are complicating issues that need to be considered. The first is the issue that the size of the measurement probe, *R*-3MCHO, is comparable to the size of the step and kink features on the surfaces. More importantly, recent studies of the real structures of high Miller index Cu(643), Cu(531), and Cu(221) surface have shown that their real structures are different from those of the ideally terminated crystal. Scanning tunneling microscopy and photoemission of adsorbed Xe have been used to show that thermal roughening of the surface and of the kinked step edges, results in a distribution of adsorption sites that is significantly different from that expected on the basis of the ideal surface structure [36–38]. Equally importantly, it has been shown that the adsorption of *R*-3MCHO can also influence the distribution of sites on the surface [34]. These all suggest that while the *R*-3MCHO desorption spectra provide qualitative insight into the types of adsorption sites exposed by the high Miller index Cu surfaces they are of limited value in quantitative determination of site densities.

The real goal of the work presented has been to demonstrate enantioselective adsorption of *R*-3MCHO on the chiral surfaces vicinal to Cu(110). In this study, these have been Cu(13,9,1)$^{R\&S}$ and Cu(651)$^{R\&S}$. Comparisons of the desorption temperatures of *R*-3MCHO from the kink sites on these surfaces reveals true enantiospecific adsorption and enantiospecific differences in the *R*-3MCHO desorption energies from the two enantiomers of a given chiral surface. The differences in the *R*-3MCHO desorption temperatures between the two enantiomers of both surfaces are $\Delta T_p = -2.4 \pm 0.8$ K on Cu(13,9,1)$^{R\&S}$ and $\Delta T_p = 2.4 \pm 0.7$ K on Cu(651)$^{R\&S}$. These correspond to a difference in desorption energies of $\Delta\Delta E_{des} = 0.7 \pm 0.2$ kJ/mol, as estimated using the Redhead equation for first-order desorption with a pre-exponential factor of 10^{13} s^{-1} [39]. A key observation, however, is that the enantiospecificity changes sign in the sense that *R*-3MCHO adsorbs preferentially on Cu(651)^{S} over Cu(651)^{R} but preferentially on Cu(13,9,1)^{R} over Cu(13,9,1)^{S}.

The simplest testable hypothesis regarding the enantioselectivity of the naturally chiral surfaces is that it is simply dictated by the chirality of the surface. In this scenario, the enantioselective preference for adsorption of a chiral probe such as *R*-3MCHO would be predictable based only on the chirality of the surface, as determined by convention from the relative orientation of the (111), (110) and (100) microfacets forming the chiral kinks. The observations made in this work clearly indicate that this hypothesis is false. This means that the enantiospecificity is dictated by the details of the surface structure and not just the orientation of the three low Miller index microfacets forming the chiral kinks sites. Given the very small enantiospecific energy differences (<1 kJ/mol), perhaps this is not surprising; it is much smaller than the adsorption energy differences between other structural features such as the differences between adsorption at kinks, steps and terraces. In particular, the desorption temperatures from the different kink sites on the Cu(651), Cu(430) and Cu(13,9,1) surfaces differ by $\Delta T_p \sim 20$ K (Fig. 4) which is much more than the enantiospecific difference in desorption

temperatures ($\Delta\Delta T_p \sim 2.4$ K) on either of the chiral surfaces. Thus, it is not surprising that the sign of the enantiospecificity of the desorption energy is influence to a greater extent by the structural details of the kink adsorption sites than by the orientation of the (111), (110) and (100) microfacets that dictate the chirality of the kinks.

5 Conclusions

R-3MCHO is an excellent probe of adsorption site types on the high Miller index Cu surfaces. In typical TPD experiments during heating at 1 K/s, *R*-3MCHO desorption peaks occur in the temperature ranges 360–385 K from the kinks, 335–350 K from the straight close-packed step edges, and 200–275 K from flat close-packed terraces. Phenomenologically, *R*-3MCHO desorption suggests that the Cu(110) surface should be considered stepped rather than flat and that the Cu(430) surface should be considered kinked rather than stepped. Adsorption of *R*-3MCHO is enantiospecific on the chiral Cu(13,9,1)$^{R\&S}$ and Cu(651)$^{R\&S}$ surfaces. The enantiospecific desorption energy differences are of opposite sign on the two pairs of surfaces and thus, are dependent on details of the surface. The enantiospecific desorption energies are sensitive to details of surface structure other than just the rotational orientation of the three low Miller index microfacets around the chiral kink sites.

Acknowledgment The authors would like to acknowledge support from the US DOE through grant number DE-FG02-03ER15472.

References

1. Polastro E (1995) Commercial outlook for chirality. Quo vadis? In: Jannes G, Dubois V (eds) Chiral reactions in heterogeneous catalysis. Plenum Publications, New York, p 5
2. Stinson SC (2001) Chiral pharmaceuticals. Chem Eng News 78:55–79
3. Stinson SC (2000) Chiral drugs. Chem Eng News 78(43):55–78
4. Zaera F (2008) Chiral modification of solid surfaces: a molecular view. J Phys Chem C 112(42):16196–16203
5. Baiker A (1997) Progress in asymmetric heterogeneous catalysis: design of novel chirally modified platinum metal catalysts. J Mol Catal A 115(3):473–493
6. Izumi Y (1983) Modified Raney-nickel (Mrni) catalyst—heterogeneous enantio-differentiating (asymmetric) catalyst. Adv Catal 32:215–271
7. Mallat T, Orglmeister E, Baiker A (2007) Asymmetric catalysis at chiral metal surfaces. Chem Rev 107(11):4863–4890
8. McFadden CF, Cremer PS, Gellman AJ (1996) Adsorption of chiral alcohols on "chiral" metal surfaces. Langmuir 12(10):2483–2487
9. Sholl DS, Asthagiri A, Power TD (2001) Naturally chiral metal surfaces as enantiospecific adsorbents. J Phys Chem B 105(21): 4771–4782
10. van Hove MA, Somorjai GA (1980) New microfacet notation for high-miller-index surfaces of cubic materials with terrace, step and kink structures. Surf Sci 92(2–3):489–518
11. Horvath J, Kamakoti P, Koritnik A, Sholl DS, Gellman AJ (2004) Enantioselective separation on a naturally chiral surface. J Am Chem Soc 126(45):14988–14994
12. Horvath JD, Baker L, Gellman AJ (2008) Enantiospecific orientation of R-3-methylcyclohexanone on the chiral Cu(643)(R/S) surfaces. J Phys Chem C 112(20):7637–7643
13. Horvath JD, Gellman AJ (2002) Enantiospecific desorption of chiral compounds from chiral Cu(643) and achiral Cu(111) surfaces. J Am Chem Soc 124(10):2384–2392
14. Horvath JD, Gellman AJ (2003) Naturally chiral surfaces. Top Catal 25(1–4):9–15
15. Ahmadi A, Attard G, Feliu J, Rodes A (1999) Surface reactivity at "chiral" platinum surfaces. Langmuir 15(7):2420–2424
16. Attard GA, Ahmadi A, Jenkins DJ, Hazzazi OA, Wells PB, Griffin KG, Johnston P, Gillies JE (2003) The characterisation of supported platinum nanoparticles on carbon used for enantioselective hydrogenation: a combined electrochemical—STM approach. ChemPhysChem 4(2):123–130
17. Attard GA, Harris C, Herrero E, Feliu J (2002) The influence of anions and kink structure on the enantioselective electro-oxidation of glucose. Faraday Discuss 121:253–266
18. Bhatia B, Sholl DS (2005) Enantiospecific chemisorption of small molecules on intrinsically chiral Cu surfaces. Angew Chem Int Ed 44(47):7761–7764
19. Gellman AJ, Horvath JD, Buelow MT (2001) Chiral single crystal surface chemistry. J Mol Catal A 167(1–2):3–11
20. Greber T, Sljivancanin Z, Schillinger R, Wider J, Hammer B (2006) Chiral recognition of organic molecules by atomic kinks on surfaces. Phys Rev Lett 96(5):056103
21. Horvath J, Kamakoti P, Koritnik A, Sholl DS, Gellman AJ (2004) Enantioselective separation on a naturally chiral surface. J Am Chem Soc 126(45):14988–14994
22. Horvath JD, Gellman AJ (2001) Enantiospecific desorption of R- and S-propylene oxide from a chiral Cu(643) surface. J Am Chem Soc 123(32):7953–7954
23. Horvath JD, Gellman AJ, Sholl DS, Power TD (2000) Enantiospecific properties of chiral single crystal surfaces. In: Hicks JM (ed) Chirality: physical chemistry, San Francisco, 2002. ACS Publications, San Francisco, pp 269–282
24. Huang Y, Gellman AJ (2008) Enantiospecific adsorption of (R)-3-methylcyclohexanone on naturally chiral Cu(531)(R&S) surfaces. Catal Lett 125(3–4):177–182
25. Power TD, Sholl DS (1999) Enantiospecific adsorption of chiral hydrocarbons on naturally chiral Pt and Cu surfaces. J Vac Sci Technol A 17(4):1700–1704
26. Rampulla DM, Francis AJ, Knight KS, Gellman AJ (2006) Enantioselective surface chemistry of R-2-bromobutane on Cu(643)(R&S) and Cu(531)(R&S). J Phys Chem B 110(21): 10411–10420
27. Schunack M, Laegsgaard E, Stensgaard I, Johannsen I, Besenbacher F (2001) A chiral metal surface. Angew Chem Int Ed 40(14): 2623–2626
28. Sholl DS (1998) Adsorption of chiral hydrocarbons on chiral platinum surfaces. Langmuir 14(4):862–867
29. Sholl DS, Gellman AJ (2009) Developing chiral surfaces for enantioselective chemical processing. AIChE J 55(10): 2484–2490
30. Sljivancanin Z, Gothelf KV, Hammer B (2002) Density functional theory study of enantiospecific adsorption at chiral surfaces. J Am Chem Soc 124(49):14789–14794
31. Zhao XY, Perry SS (2004) Ordered adsorption of ketones on Cu(643) revealed by scanning tunneling microscopy. J Mol Catal A 216(2):257–262
32. Attard GA (2001) Electrochemical studies of enantioselectivity at chiral metal surfaces. J Phys Chem B 105(16):3158–3167

33. Jenkins SJ, Pratt SJ (2007) Beyond the surface atlas: a roadmap and gazetteer for surface symmetry and structure. Surf Sci Rep 62(10):373–429
34. Zhao XY, Perry SS, Horvath JD, Gellman AJ (2004) Adsorbate induced kink formation in straight step edges on Cu(533) and Cu(221). Surf Sci 563(1–3):217–224
35. Somorjai GA, Li Y (2010) Introduction to surface chemistry and catalysis, 2nd edn. Wiley, New York
36. Baber AE, Gellman AJ, Sholl DS, Sykes ECH (2008) The real structure of naturally chiral Cu{643}. J Phys Chem C 112(30): 11086–11089
37. Baker L, Holsclaw B, Baber AE, Tierney HL, Sykes ECH, Gellman AJ (2010) Adsorption site distributions on Cu(111), Cu(221), and Cu(643) as determined by Xe adsorption. J Phys Chem C 114(43):18566–18575
38. Clegg ML, Driver SM, Blanco-Rey M, King DA (2010) Atomic roughness of an intrinsically chiral surface orientation of an fcc metal: Cu{531}. J Phys Chem C 114(9):4114–4117
39. Redhead PA (1962) Thermal desorption of gases. Vacuum 12: 203–211